# Analyses about parameters that affect cyclic variation in a spark ignition engine

Enzo Galloni

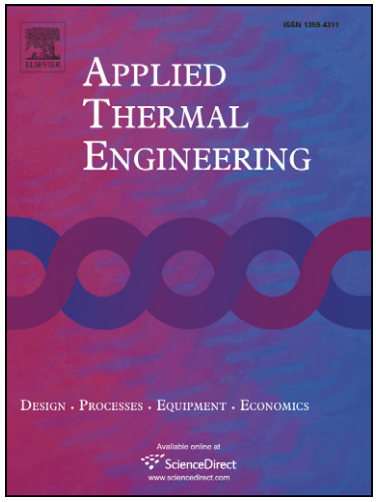


# Analyses about parameters that affect cyclic variation in a spark ignition engine

Enzo Galloni

PII: S1359-4311(08)00262-7
DOI: 10.1016/j.applthermaleng.2008.06.001
Reference: ATE 2532

To appear in: *Applied Thermal Engineering*

Received Date: 28 May 2007
Revised Date: 26 March 2008
Accepted Date: 2 June 2008

Please cite this article as: E. Galloni, Analyses about parameters that affect cyclic variation in a spark ignition engine, *Applied Thermal Engineering* (2008), doi: 10.1016/j.applthermaleng.2008.06.001

# Analyses about parameters that affect cyclic variation in a spark ignition engine

*Enzo Galloni*[*]

*Department of Industrial Engineering– University of Cassino*

## Abstract

The combustion stability of a small spark-ignition engine has been investigated by means of both experimental tests and numerical analyses. The cyclic variation in combustion has been measured at part load considering several combustion chamber geometries. For each considered operating point, the in cylinder phenomena characterizing the engine have been reproduced by CFD analysis performed by means of a RANS approach. The properties of the mean flow calculated in the spark region at the spark time seem to affect the extent of the measured cyclic dispersion. In particular, for the investigated engine, the measured coefficient of variation in the indicated mean effective pressure seems correlated with both the calculated mean laminar flame speed and the calculated mean turbulence intensity.

Keywords: S.I engine, Cyclic variation, CFD analyses, RANS approach

## Nomenclature

| | |
|---|---|
| BMEP | Brake mean effective pressure [bar] |
| COV | Coefficient of variation: the standard deviation in IMEPh divided by the mean IMEPh [%] |
| EGR | Calculated mean residual gas mass fraction in the spark region at the spark time [-] |
| IMEPh | Indicated mean effective pressure calculated by considering only the work delivered to the piston over the compression and expansion strokes [bar] |
| k | Calculated mean turbulent kinetic energy density [$m^2/s^2$] |
| $l_i$ | Integral length scale ($l_i = 0.09^{3/4} k^{3/2}/\varepsilon$) [m] |

[*] Corresponding author. Tel +39 776 2994005; fax: +39 776 2994365.

E-mail address: galloni@unicas.it

| | |
|---|---|
| $l_k$ | Kolmogorov length scale [m] |
| $Re_T$ | Turbulent Reynolds number [-] |
| $S_l$ | Calculated mean laminar flame speed in the spark region at the spark time [m/s] |
| u' | Calculated mean turbulence intensity, considered isotropic, in the spark region at the spark time (u'=$\sqrt{2/3 \cdot k}$ ) [m/s] |
| U | Magnitude of the calculated mean flow velocity in the spark region at the spark time [m/s] |
| ε | Calculated mean turbulent kinetic dissipation rate [$m^2/s^3$] |
| ϕ | Calculated mean air fuel equivalence ratio in the spark region at the spark time [-] |
| $\tau_k$ | Kolmogorov time scale [s] |
| $\tau_m$ | Turbulent mixing time [s] |

## 1. Introduction

Today, engine designers are seeking every kind of solution aimed at the reduction of fuel consumption and emission levels.

Cycle by cycle variation in combustion significantly influences the performance of spark-ignition engines [1, 2].

In a spark-ignition engine the operating spark timing is set for the average cycle, thus the cycles that burn faster than average have effectively over advanced spark-timing, while the slow burning cycles are ignited too late. Only a few cycles burn with the optimum spark-timing, thus resulting in a loss of power and efficiency.

The extremes of the cyclic dispersion limit engine operation. The fastest burning cycles, which are ignited too early, are most likely to knock at full load; these cycles determine the use of a higher octane rating or an engine with a lower compression ratio. At partial load, the slowest burning cycles are most likely to burn incompletely, determining an unacceptable loss of efficiency and high levels of unburnt hydrocarbons. As the mixture becomes leaner with excess air or more diluted with a higher exhaust gas residual fraction, the cycle to cycle dispersion increases, thus these cycles determine the lean mixture limits or the amount of exhaust gas recirculation which the engine can tolerate. Finally, variations in combustion lead to different amounts of work per cycle correlated with fluctuations in the engine speed, or its torque output, which directly relate to vehicle driveability.

If cyclic dispersion could be eliminated, the engine efficiency could be largely increased especially when it operates with weak mixtures [2].

It is widely accepted that the early flame development deeply influences the subsequent combustion phase [3]. Many authors [2, 4, 5] consider the ignition delay stage as the most important phase for the overall cyclic dispersion in the engine performance.

The formation of the flame kernel and the following flame growth through a laminar like phase depend on: the local air fuel ratio, the mixture motion and the exhaust gas concentrations in the spark plug gap at the time of ignition and in the spark plug region immediately after ignition.

Cyclic variations occur because the bulk flow, turbulence, residual amounts and gasoline supplied to each cylinder vary from cycle to cycle. Moreover, within the cylinder, the mixing of air fuel and exhaust gas residuals is not complete, therefore the mixture is not homogeneous at the spark time. The turbulent nature of the flow in the cylinder causes random spatial and time-dependent fluctuations in the variables characterising the mixture and its flow field. These fluctuations cause a random value of the mixture concentration in the spark plug region, a random convection of the spark kernel away from the electrodes, a random heat transfer from the burning kernel, etc.[5, 6, 7]. In particular, the random displacement of the flame kernel during the early stages of combustion seems to play a major role in the origination of cycle variation in combustion [8].

Moreover, even if many factors do not cause cyclic variation, they determine the sensitivity of the engine to the factors which give origin to the phenomenon. For example, the overall weakness of the mixture [9,10,11,12], the spark plug and the spark-timing [13,14] and the in cylinder mixture motion [15,16,17] do not cause cyclic dispersion in combustion themselves but affect the extent of cyclic variation caused by other factors. The conclusion seems to be that anything that tends to slow down the flame propagation process, especially in its development stage, tends to increase the cyclic dispersion in combustion.

The numerical modeling of the complex phenomena taking place in the S.I. engine gives rise to a lot of data which are difficult to achieve using experimental tests; CFD calculations have become a very useful tool in improving the knowledge of phenomena and in indicating specific optimal solutions regarding engine turbulent flows. The purpose of this paper is to verify if the results obtained from Reynolds Averaged

Numerical Simulations could supply useful information in foreseeing the extent of cycle variation occurrence in a spark-ignition engine.

A small spark-ignition engine has been tested by changing the combustion chamber shape in a few operating points at part load. The engine behavior has been simulated by means of CFD calculations. Of course these numerical analyses cannot provide information about cyclic fluctuations, but CFD simulations have been used to calculate the mean value in the ignition zone at the ignition time of the main features that affect the early stages of flame development.

## 2. Experimental Approach

A spark-ignition engine using three different shapes of the combustion chamber has been considered.

The engine features four cylinders (total piston displacement 1368 $cm^3$) and two vertical valves per cylinder. The fuel is introduced upstream the inlet valves by means of plate four hole injectors capable of producing droplets with a Sauter mean diameter of about 130 μm.

Almost half of the combustion chamber is realized inside the cylinder head. In Figure 1, the three geometries, called Geo A, Geo B and Geo C, have been reported. They are characterized by decreasing values of both the squish area and the volumetric compression ratio (Table 1). The squish area is concentrated on the opposite side of the spark-plug and it has been varied by modifying the portion of the engine head close to the exhaust valve. As can be observed in Figure 2, relatively high squish area values have been obtained by carefully avoiding masking the inlet valve, in order not to penalize the engine volumetric efficiency.

To measure the cycle by cycle variations, the engine has been coupled to an eddy current dynamometer. Measurements have been taken in agreement with the European Standard UNI ISO 3046.

An AVL Puma 5.3 system has been used for test control and data acquisition. The fuel consumption has been measured by a fuel balance (accuracy less than 0.5%), while a Horiba UEGO sensor has been used to measure the air excess ratio (accuracy less than 4%) . A high pressure miniaturised quartz transducer (AVL GM12D) has been located in the head of the first cylinder, while a crankshaft encoder (AVL 364) has given the crank angle reference for the measurements. A pc with an AVL Indimeter 619 card controlled the acquisitions matching the pressure signals with the encoder signal. An AVL ignition time module 3080 has been used to measure the spark angle.

For each geometry, spark advance has been adjusted to MBT, the air-fuel ratio has been set stoichiometric. The mixture has been formed by an open valve injection that starts at the top dead center of the suction stroke.

Three measurements have been done in the operating points shown in Table 2; in each measurement 700 engine cycles with a 0.5 crank angle sampling frequency have been acquired. Data has been measured only when the exhaust gas temperature was constant. As a measure of cyclic variability, the coefficient of variation in indicated mean effective pressure has been derived from pressure data. To highlight the effect of the cyclic variation in combustion, only the work delivered to the piston over the compression and expansion strokes has been considered; therefore the coefficient of variation is calculated like the standard deviation of the indicated mean effective pressure (IMEPh) calculated between the intake valve closing and the exhaust valve opening, divided by the mean IMEPh (Eq.1).

$$COV = \frac{\sigma_{IMEPh}}{IMEPh} \times 100 \qquad (1)$$

The results obtained for each head shape are shown in Table 3. They are the mean values calculated on the basis of the three different measurements done for each operating point. In each considered case the difference between the acquired COVs and the relative mean value is less than 4%.

The measured COV is always less than 5%, i.e. less than the upper limit tolerated in power generation and for driveability reasons in automotive applications. As usual the higher COV have been measured when the engine runs at minimum load.

## 3. Numerical Approach

Multidimensional numerical techniques, in which the complex phenomena taking place in an engine are solved by using a space-resolved numerical technique, have become an essential tool in improving the knowledge of phenomena and in indicating specific optimal solutions.

The Direct Numerical Simulations (DNS) approach allows solving the full Navier-Sokes equations by computing all the turbulence scales explicitly. In this sense, DNS appear as exact numerical experiments which are able to reproduce the finest details of turbulence and turbulence-related phenomena [7]. Unfortunately, according to the equilibrium theory of Kolmogorov, grid spacing and time steps, capable of following the vortex dynamic in the spatio-temporal development of turbulent flows, should be

proportional to $N_j = l_i / l_k \propto Re_T^{3/4}$ for the length scale and $N_t = \tau_m / \tau_k \propto Re_T^{1/2}$ for the time scale. In the internal combustion engine, $Re_T \approx 10^4$ [1], so $N_j$ and $N_t$ are on the order of $10^3$ and $10^2$; considering that any turbulent flow is intrinsically tri-dimensional and unsteady, due to excessive computer requirements, the DNS method is inapplicable in solving turbulent flows in boxes of size comparable to the engine combustion chambers.

In many applications, engineers are interested only in the averaged mean field and its effect and consequences; by decomposing the instantaneous property into a mean value and fluctuations around the mean, in accordance with the Reynolds approach, the average flow field can be described by resolving the balance equations in a mediate form (Reynolds Averaged Navier-Stokes equations). Unfortunately, because of the non-linear convective terms, this operation results in an increase of unknown variables relate to the so called turbulent fluxes; this highlights the loss of information due to averaging. Consequently, this approach needs a pre-determined turbulent model which is able to translate the undescribed sub-grid phenomena into a set of equations so as to perform the mathematical closure of the problem. The type and the number of auxiliary equations define the closure level. Two levels of approach are mainly used: eddy viscosity models (first-order) and Reynolds stress models (second order). The second-order models solve a differential transport equation for each component of the turbulent flux; some variants of the Reynolds-stress models have been used for real industrial applications [18], nevertheless many CFD users prefer less complicated and more robust solutions. The first-order models assume that the turbulent flux of momentum, heat, and species is directly related to the mean flow field via the Bousinnesq hypothesis. Many eddy viscosity models have been proposed during the last three decades (k-ω [19], ζ-f [20], Spalart-Allmaras [21] ect.), but the most popular approach remains the k-ε model proposed first from Launder and Spalding [22]. The k-ε model considers the turbulence like isotropic; turbulent kinetic energy and turbulent dissipation rate are calculated by means of two balance equations coupled with the general governing equations.

Despite the various modifications proposed to extend the validity of this model (the RNG theory [23] as example), the limits of the k-ε approach are well know; in particular the little accuracy in solving flows with separated or curved streamline, bulk compression etc. [24]. Besides, the obtained results depend on the values assigned to the various empirical constants that appear in the turbulent model; often setting of these

constants is not clearly established [24, 25]. Nevertheless, considering its stability, computational speed and general applicability to a wide range of flows, the k-ε model remains a good compromise between calculation efficiency and accuracy of the solution.

Although large-eddy simulation techniques are becoming more viable as computing power increases [26], the k-ε model (i.e. the first order approach) is likely to remain the more used approach by the industrial researches [25].

The numerical approach adopted in this paper has been described in detail in [27, 28]. Briefly, CFD simulations, which reproduce the suction stroke and the subsequent compression stroke, have been performed by means of the 7.3 standard release of the 3-D AVL FIRE code [29,30,31]. The processor allows solving the ensemble-averaged governing equations of the flow and the heat transfer within the computational domain. The partial differential transport equations are discretized on the basis of a finite volume method.

The problem of the unknown turbulence correlation is resolved through a k-ε approach. To take into account the non-uniformity of the mixture concentration characterizing the port injection engines, a spray model is used to simulate the mixture formation. This model is based on the well-established Lagrangian discrete droplet method [32].

This solves ordinary differential equations for the trajectory, momentum, heat and mass transfer of single droplets, each being a member of a group of identical non-interacting droplets (parcel). Thus, one member of the group represents the behaviour of the complete parcel; trajectory and velocity of the droplet parcel are calculated by means of the Newton law considering the action of both the drag force and the gravitational force. The spray behaviour is calculated considering evaporation, turbulent dispersion, wall interaction and break-up phenomena.

The O'Rourke [33] method has been used to consider the turbulent dispersion caused by the interaction between droplets and turbulent eddies. The characteristic break-up time and the stable drop radius of droplets are calculated by means of the wave approach proposed in [34].

The wall interaction is based on the on the spray/wall impingement model of Naber and Reitz [35] based on a critical Weber number. The droplet diameter after the impingement is considered depending on the Weber number and is calculated according to the Walljet2 approach described in [31].

The injection rate, the spray cone and the initial distribution of the Sauter mean diameter have been assumed according to both injector characteristics and fuel supply pressure.

The combustion chamber and the intake port have been meshed for each geometry. Dynamic grids, which are able to follow piston and valve movements, have been generated using hexahedral cells. They have about 25000 cells as a minimum and about 130000 cells as a maximum (Figure 2).

Mesh distribution has been defined thus to produce cells as regular-shaped and orthogonal as possible, even though engine geometry do not allow to obtain the right grid quality in the whole domain. The greatest care was used to well reproduce the exact surface geometry and to correctly discretize the valve gap during the valve movement. The mean grid resolution has been chosen considering that the numerical solution of the Navier-Stokes equations becomes more and more accurate if the grid is refined, but considering also that the Lagrangian liquid phase approach is based on the assumption that the volume of the liquid droplets inside the cell must be very small compared to the cell volume.

Initial and boundary conditions for engine simulations have been evaluated by means of 1-D, unsteady computations running separately from the 3-D code. The charge within the cylinder has been considered initially quiescent and homogeneous. At inflow boundary the mass flow rate and the temperature are set; no velocity profiles are assigned. The integral length scale is assumed equal to 10% of the hydraulic diameter, while the inlet turbulent kinetic energy is set equal to the square of 10% of the inlet mean velocity provided by the 1-D model. The boundary conditions at solid walls are the no-slip velocity and the constant temperature conditions.

Runs have been done with a fixed time step equivalent to 0.2 crank angle degrees.

For flow modeling validation steady calculations have been carried out by reproducing the experimental tests used for engine ports characterization: calculations show discharge coefficients very close to those measured in the experimental tests. With regard to transient simulations, the calculated mass of the air-fuel mixture trapped in the cylinder practically coincides with the measured data. More details about modeling validation are described in [36]; as example, figure 3 shows some comparison between calculated and measured data.

## 4. MODELING RESULTS

By means of CFD calculations the ensemble-average values of the residual gas mass fraction (EGR), the gaseous air-fuel equivalence ratio (ϕ), the turbulent intensity (u') and the other features of the charge in the ignition zone have been calculated at the spark time.

In particular, the mean values in a 5 mm radius sphere, centered at the spark-plug, have been considered. The size of the control sphere has been chosen considering both the size of the spark-plug electrodes and the need to have a meaningful number of cells, about 75, in order to average out the considered parameters. However a sensitivity study has been performed considering both a sphere radius equal to 3 mm and a sphere radius equal to 7.5 mm; the differences between the calculated mean values range from 0% to 8%. The larger difference has been found relatively to the velocity magnitude calculated for the GEOC, 1500@1 case.

The calculated mean values are shown in Table 4.

Temperature and pressure are very different for the considered test cases according to the adopted spark timing. Turbulent intensity and mean velocity depend on the engine speed. For the 2000@2 and 3000@3 cases the magnitude of the calculated mean velocity is within the range of 3-5 m/s that in [38] is suggested as large enough to move the kernel away from the electrodes, but as insufficient to quench it by stretching; the 1500@1 cases show a mean velocities less than 2 m/s. About the integral length scale, there are not meaningful differences between the considered cases.

At the spark time the distribution of both the residual gas and the fuel vapor concentration in the cylinder is non homogenous (figure 4).

At 1500 rpm and BMEP equal to 1 bar, the spray behavior causes rich mixtures in the spark plug zone for each considered geometry, even though the engine is running with an overall stoichiometric mixture; instead a 3000 rpm and BMEP equal to 3 bar lean mixtures have been calculated in the spark region.

In Figure 5 the measured covariance of IMEPh has been plotted versus the air equivalence ratio, the turbulent intensity and the mean velocity calculated in the spark region at the spark time.

It is worth to notice that the cases characterised by the higher values of measured coefficient of variation in IMEPh show:

- calculated equivalence ratios do not close to the stoichiometric value. This is reasonable because the highest burning speed is achieved in stoichiometric or slightly enriched mixtures;
- the lower calculated turbulent intensities. Actually, this trend agrees with several studies in which it has been shown that increasing reasonably the level of turbulent kinetic energy allows obtaining quick flame kernel growth and consequently improve the combustion stability [6,16];
- mean velocities outside the range that in [38] is suggested as optimal to minimize the combustion dispersion.

Considering that cyclic variation is increased by anything that tends to slow down the early combustion process, it is interesting to evaluate the behavior of the laminar flame speed calculated in the spark zone at the spark time.

The laminar burning velocity is an intrinsic property of the mixture and it is a function of the equivalent ratio, pressure and temperature of the reactants. For a gasoline-air mixture diluted by the exhaust, the laminar flame speed is calculated according to [1]:

$$S_l(\phi, p, T, egr) = S_l(\phi, p, T) \cdot (1 - 2.06 \cdot \gamma^{0.77}) \quad (2)$$

where $\gamma$ is the mole fraction of diluent burnt gas. $S_l$ is calculated by means of equation (3), with $\alpha$ and $\beta$ depending on the equivalence air-gasoline ratio (equations (4), (5)), while $S_{l0}$ approximates the laminar flame speed at reference conditions (equation (6)).

$$S_l(\phi, p, T) = S_{l_0}(\phi) \cdot \left(\frac{T}{298}\right)^{\alpha} \cdot \left(\frac{p}{101000}\right)^{\beta} \quad (3)$$

$$\alpha = 2.4 - 0.271 \cdot \phi^{3.51} \quad (4)$$

$$\beta = -0.357 + 0.14 \cdot \phi^{2.77} \quad (5)$$

$$S_{l_0}(p_0, T_0) = 35 - 110 \cdot (\phi - 1.125) \quad (6)$$

In table 5 are shown the calculated values of $S_l$.

By plotting the measured COV in IMEPh versus the calculated laminar flame speeds (figure 6), it is possible to see that the lower coefficients of variation are associated with the higher laminar speed burning. Actually, this is reasonable considering that the quick flame development stage (when the burning velocity is close to its laminar value) tends to decrease the influence of random variation in the thermo-chemical fluid properties reducing the cyclic variation.

Disregarding the cyclic fluctuations characterizing the engine operating, in the following a mathematical relationship between the measured coefficient of variation in IMEPh and the mean values calculated by the CFD approach has been sought.
RANS calculations allow to appreciate the mean value of the laminar flame speed to consider the influence of the termochemical properties of the charge, while the flow field influence can be considered by means of the mean flow velocity, the mean turbulence intensity and the mean value of the integral length scale. As the calculated length scale do not show meaningful differences between the considered cases, this parameter has been neglected.
Considering the laminar flame speed, the magnitude of the mean velocity and the turbulent intensity in the spark region at the spark time as factors that affect the turbulence occurrence, it has been assumed that the coefficient of variation in IMEPh could be described by means of the following relationship:

$$COV = c \cdot S_l^{\,x} \cdot u'^{y} \cdot U^{z} \qquad (7)$$

where c, x, y and z are unknowns. Equation 7 can be written as:

$$\log(COV) = \log(c) + x \cdot \log(S_l) + y \cdot \log(u') + z \cdot \log(U) \qquad (8)$$

Equation 8 has been solved by means of a multiple linear regression over the whole set of calculated data; the following mathematical law has been obtained by using the method of least squares:

$$COV(S_l, U', U) = 10^{0.24} \cdot S_l^{\,-0.49} \cdot u'^{-0.31} \cdot U^{-0.06} \qquad (9)$$

The correlation index found is: $R^2$=0.61; according to [39], it has been calculated by considering:

$$R^2 = 1 - \frac{\sum_j \left(COV_j - COV(S_{l\,j}, u'_j, U_j\right)^2}{\sum_j \left(COV_j - COV_M\right)^2} \qquad (10)$$

where $COV_M$ is the mean value of the measured coefficients of variation, while the subscript j refers to each examined cases.
The correlation index is not high; but equation 9 considers only the parameters, appreciable by means RANS analyses, that affects the cyclic variation of the engine. The cyclic fluctuations that determine this phenomenon are not considered. In such sense the equation 9 seems to explain about the 60% of the measured cyclic variation. Despite the calculated value of the correlation index is not high, the deviation between calculated and measured data is acceptable; the maximum error is 20% with regard to Case 3000@3, GEOA; the mean error is less than 10%.

Figure 7 shows a comparison between the measured and estimated data for the considered test cases. Equation 9 seems to provide satisfactory qualitative predictions of the coefficient of variation in IMEP for these geometries in these operating points. In particular, this relationship highlights the influence of the considered parameters on the phenomenon. The cyclic variation decreases when either the laminar flame speed or the turbulent intensity increase, while it is slightly affected by the mean velocity.

Cyclic fluctuations occur during the whole combustion process. In each point of the combustion chamber, the mean factors that determine the local burn rate will change randomly from cycle to cycle causing local rise or local decrease of the flame speed. During the turbulent combustion phase, large flames will be able to integrate these local fluctuations of the burn rate; instead, during the early stage of the combustion, both the flame kernel or the small flame do not have the chance of averaging out these random occurrences.

For the three geometries, the higher COVs have been measured when the engine runs at minimum load. Correspondently in the spark-zone at the spark time, the minimum values for both the laminar flame speed and the turbulence intensity have been calculated. In this case the flame kernel grows slowly, thus it is more subject to the cyclic fluctuation occurrence.

At 2000 rpm and BMEP equal to 2 bar, the cyclic variation decreases because of the rising of both the laminar flame speed and turbulence intensity that make faster the early part of combustion.

At 3000 rpm and BMEP equal to 3 bar, the mixtures do not close to the stoichiometric value slowdown the laminar flame speed in the spark-zone at spark-time, especially for the GEO C geometry. For the GEO A and GEO B geometries, the large rising of the turbulent intensity seems to be able to overcome this occurrence producing a yet more stable combustion.

## 5. Conclusions

Although the RANS approach does not allow to grasp the causes which determine combustion instability, it allows to investigate the factors which influence the extent of cyclic variation in the internal combustion engine.

With regard to the engines investigated in this paper, CFD calculations show that the operating points characterized by high cyclic dispersion are characterized by mixtures do not close to the stoichiometric values, low turbulent kinetic energies and very low charge velocities in the spark region at the spark time.

The laminar flame speed, turbulence intensity and velocity magnitude have been considered among the factors that affect the extent of the engine cyclic variation. The influence of these parameters has been investigated.

Correlating these features of the charge with the measured coefficient of variation in the indicated mean effective pressure, a mathematical relationship has been obtained by means of a multiple regression.

This relationship highlights the influence of the considered factors on the extent of the cyclic variation measured in the considered cases: increasing both the laminar flame speed and the turbulence intensity, in the spark-zone at the spark-time, the coefficient of IMEPh decreases; in the considered cases the mean charge velocity slightly affects the phenomenon.

Actually, considering the weight of the early stage of the combustion, the calculated mean values of both the laminar flame speed and the turbulence intensity explain the trends of the measured COVs.

Therefore the analysis described in this paper seems to be able to provide guidelines for reducing the cyclic variation of the engine under examination. Thus RANS calculations can be an important tool in indicating optimal solutions regarding the development of this engine in using high EGR ratio or very lean mixtures, i.e. in operative conditions where the combustion stability determines the weak mixture limit tolerable by the engine.

## References

1. J.B. Heywood, Internal combustion engine fundamentals, McGraw-Hill Book Co.,1988
2. R. Stone, Introduction to internal combustion engines, Macmillan, Hong Kong, 1992
3. K.-H. Lee, K. Kim, Influence of Initial Combustion in SI Engine on Following Combustion Stage and Cycle-by-Cycle Variations in Combustion Process, International Journal of Automotive Technology, Vol.2, N.1, pp 25-31, 2001
4. T. Mantel, Three dimensional study of flame kernel formation around a spark plug, SAE Paper n. 920587, 1992
5. B. Johansson, Cycle to Cycle Variations in SI Engines – The Effects of Fluid Flow and Gas Composition in the Vicinity of the Spark Plug on Early Combustion, SAE Paper N. 962084, 1996

6. N. Ozdor, M. Dulger and E. Sher, Cyclic Variability in Spark Ignition Engines. A Literature Survey, SAE Paper n. 940987, 1994
7. T.A. Baritaud, Optical and Numerical Diagnostic for SI Engine Combustion Studies, Proceedings of International Symposium COMODIA, 1994
8. C.R. Stone, A.G. Brown and P. Beckwith, Cycle-by-Cycle Variations in Spark Ignition Engine Combustion – Part II: Modelling of Flame Kernel Displacements as a Cause of Cycle-by-Cycle Variations, SAE Paper n. 960613, 1996
9. P.G. Hill, Cyclic Variation and Turbulence Structure in Spark-Ignition Engines, Combustione and Flame, 72,pp. 73-89, 1988
10. M.B. Young, Cyclic Dispersion in the Homogeneous-Charge Spark-Ignition – A Literature Survey, SAE Paper n. 810020, 1981
11. N. Nedunchezhian, S. Dhandapani, Experimental Investigation of Cyclic Variation and Combustion Phases in a Lean-Burn, Two-Stroke SI Engine, SAE Paper N. 2001-28-0059, 2001
12. K. Kampanis, C. Arcoumanis, R. Kato and S. Kometani, Flow, Combustion and Emissions in a Five-Valve Research Engine, SAE Paper n. 2001-01-3556, 2001
13. A.G. Brown, C.R. Stone and P. Beckwith, Cycle-by-cycle variations in Spark Ignition Engine Combustion – Part I: Flame Speed and Combustion Measurements, and a simplified Turbulent Combustion Model, SAE Paper n.960612, 1996
14. S. Pishinger and J.B. Heywood, A Study of Flame Development and Engine Performance with Breakdown Ignition Systems in a Visualization Engine, SAE Paper n. 880518, 1988
15. J.F. Le Coz, Cycle-to-Cycle Correlations between Flow Field and Combustion Initiation in an S.I. Engine, SAE Paper n. 920517, 1992
16. W. Cartellieri, F.G. Chmela, P.E. Kapus and R.M. Tatschl, Mechanisms Leading to Stable and Efficient Combustion in Learn Burn Gas Engines, Proceedings of International Symposium COMODIA, 1994
17. S. Pischinger and J.B. Heywood, How Heat Losses to the Spark Plug Affect Flame Kernel Development in an SI Engine, SAE Paper n. 900021, 1990
18. B. Basara, Employment of the second-moment turbulence closure on arbitrary unstructured grids, Int. J. Numerical Methods in Fluids, Vo. 44, pp. 377-407, 2004
19. D.C. Wilcox, Reassessment of the scale-determining equation for advanced turbulence models, AIAA J., 1988

20. K. Hanjalic, M. Popovac and M. Hadziabdic, A robust near-wall elliptic relaxation eddy viscosity turbulence model for CFD, Int.J.Heat and Fluid Flow, 2004
21. P.R. Spalart, S.R. Allmaras, A one-equation turbulence model for aerodynamic flows, La Recherce Aerospatiale, 1994
22. B. E. Launder, D.B. Spalding, Mathematical models of Turbulence, New York: Academic Press, 1972
23. V. Yakhot, S.A. Orszag, Renormalization Group Analysis of Turbulence. I. Basic Theory, Journal of Scientific Computing, 1986
24. J.I. Ramos, Internal Combustion Engine Modelling, Hemispherer Publishing Corporation, 1989
25. P. C. Miles, B. H. RempelEwert, R. D. Reitz, Experimental Assessment of Reynolds-Averaged Dissipation Modeling in Engine Flows, Sae Paper N. 2007-24-0046, 2007
26. O. Vermorel, S. Richard, O. Colin, C. Angelberger, A. Benkenida, Predicting Cyclic Variability in a 4 Valve SI Engine Using LES and the AVBP CFD Code, International Multidimensional Engine Modeling User's Group Meeting, 2007
27. G. Fontana, E. Galloni and R. Palmaccio, "Development of a New Intake System for a Small Spark-Ignition Engine: Modeling the Flow through the Inlet Valve", SAE Paper no. 2003-01-0369, 2003
28. G. Fontana, E. Galloni, E. Jannelli and R. Palmaccio, "Influence of the Intake System Design on a Small Spark-Ignition Engine Performance. A Theoretical Analysis", SAE Paper no. 2003-01-3134, 2003
29. R. Tatschl, K. Wieser, R. Reitbauer, "Multidimensional Simulation of Flow Evolution, Mixture Preparation and Combustion in a 4-Valve SI Engine", International Symposium COMODIA 94, Yokohama, 1994
30. R. Tatschi and H. Riediger, "PDF Modelling of Stratified Charge SI Engine Combustion", SAE Paper 981464, 1998.
31. AVL FIRE Handbook, Version 7, April 2000, Internal Report.
32. J.K. Dukowicz, A Particle-Fluid Numerical Model for Liquid Sprays, Journal of Computational Physics, 35, pp. 229-253, 1980
33. P.J. O'Rourke, Statistical Properties and Numerical Implementation of a Model for Droplet Dispersion in Turbulent Gas, Journal of Computational Physics 83, 1989
34. A.B. Liu, R.D. Reitz, Modeling the Effects of Drop Drag and Breakup on Fuel Sprays, SAE Paper 930072, 1993

35. J.D, Naber, and R.D. Reitz, Modeling Engine Spray/Wall Impingement, SAE Paper 880107, 1988
36. G. Fontana, E. Galloni, R. Palmaccio, "Numerical and Experimental Analysis of Different Combustion Chambers for a Small Spark-Ignition Engine", SAE Paper N. 2004-01-1998, Tolouse, 2004
37. C. R., Choi and K. Y. Huh, "Development of a Coherent Flamelet Model for a Spark-Ignited Turbulent Premixed Flame in a Closed Vessel", Combustion and Flame, 1998
38. S. Pishinger and J.B. Heywood, How Heat Losses to the Spark Plug Affect Flame Kernel Development in a SI Engine, SAE Paper 900021, 1990
39. R.M. Bethea, B.S. Duran, T.L. Boullion, Statistical Methods, Marcel Dekker Inc., 1985

**Figure Captions**

Figure 1. Drawing of combustion chambers. Squish area for GEO A (left) and GEO C (middle); cross section for GEO B (right)

Figure 2. Geo C grid and spray behaviour during the suction stroke

Figure 3. Comparison between measured and calculated in cylinder pressure (left: Geo A, 1500@1; right: Geo C 2000@2).The combustion development has been modelled by means the Coherent Flamelet Model [37]. Tuning has been done considering the engine running at full load: the production coefficient has been set equal to 1.3, while an initial value of the flame surface density equal to 300 1/m in a spherical kernel (r=4 mm) has been considered.

Figure 4. Calculated equivalence ratio field at spark time for GEO B. Cross section through the spark zone (left: 1500@1, right: 3000@3).

Figure 5. Measured coefficient of variation in IMEP versus: the calculated air-gasoline equivalence ratio (left), the calculated mean turbulence intensity (middle) and the magnitude of the calculated mean velocity (right). Mean values are calculated in the spark zone at the spark time

Figure 6. Measured coefficient of variation in IMEP versus the calculated laminar flame speed in the spark zone at the spark time

Figure 7. Comparison between measured coefficient of variation in IMEPh and estimated coefficient of variation in IMEPh for the examined cases; estimated values are calculated by means of equation 9.

Table 1

Prototype geometric characteristics

| | Geo A | | Geo B | | Geo C | |
|---|---|---|---|---|---|---|
| Compression Ratio [-] | 11.20 | + 2.28 % | 11.10 | + 1.37 % | 10.95 | + 0.00 % |
| Squish Area [$mm^2$] | 561 | + 39.90 % | 488 | + 21.70 % | 401 | + 0.00 % |

Table 2

Test cases

| Operating point | Engine speed [rpm] | BMEP [bar] | $\phi$ [-] | Spark Advance [°] | | |
|---|---|---|---|---|---|---|
| | | | | Geo A | Geo B | Geo C |
| 1500 @1 | 1500 | 1 | 1.0 | 32.0 | 36.0 | 33.0 |
| 2000@2 | 2000 | 2 | 1.0 | 28.0 | 32.0 | 34.0 |
| 3000@3 | 3000 | 3 | 1.0 | 36.0 | 33.0 | 31.0 |

Table 3

Coefficient of variation measured in the first cylinder for the considered cases

| | | 1500@1 | 2000@2 | 3000@3 |
|---|---|---|---|---|
| COV [%] | Geo A | 1.55 | 1.19 | 0.91 |
| | Geo B | 1.45 | 1.31 | 1.09 |
| | Geo C | 1.87 | 1.34 | 1.40 |

Table 4

Mean values computed in the spark-plug region at the spark time.

| | | 1500@1 | 2000@2 | 3000@3 |
|---|---|---|---|---|
| EGR [%] | Geo A | 9.5 | 8.0 | 6.8 |
| | Geo B | 9.5 | 8.3 | 7.1 |
| | Geo C | 9.4 | 8.1 | 7.0 |
| $\phi$ [-] | Geo A | 1.32 | 1.04 | 1.0 |
| | Geo B | 1.33 | 1.07 | 0.92 |
| | Geo C | 1.31 | 1.03 | 0.87 |
| u' [m/s] | Geo A | 2.18 | 2.73 | 4.34 |
| | Geo B | 2.16 | 2.79 | 4.48 |
| | Geo C | 2.20 | 2.71 | 4.50 |
| U [m/s] | Geo A | 1.20 | 3.87 | 5.37 |
| | Geo B | 1.28 | 4.31 | 5.15 |
| | Geo C | 1.16 | 4.50 | 5.10 |
| Temperature [K] | Geo A | 629.5 | 636.0 | 595.4 |
| | Geo B | 597.6 | 601.5 | 613.5 |
| | Geo C | 624.5 | 592.5 | 631.0 |
| Pressure [Pa] | Geo A | 2.85E+5 | 3.97E+5 | 3.79E+5 |
| | Geo B | 2.36E+5 | 3.30E+5 | 4.00E+5 |
| | Geo C | 2.71E+5 | 3.13E+5 | 4.38E+5 |
| $l_i$ [m] | Geo A | 2.2E-3 | 2.0E-3 | 2.1E-3 |
| | Geo B | 2.2E-3 | 2.0E-3 | 2.1E-3 |
| | Geo C | 2.2E-3 | 2.0E-3 | 2.1E-3 |

Table 5

Mean laminar flame speed computed in the spark-plug region at the spark time.

| | | 1500@1 | 2000@2 | 3000@3 |
|---|---|---|---|---|
| Sl [m/s] | Geo A | 0.70 | 0.91 | 0.82 |
| | Geo B | 0.63 | 0.84 | 0.79 |
| | Geo C | 0.70 | 0.82 | 0.75 |

Fig.1

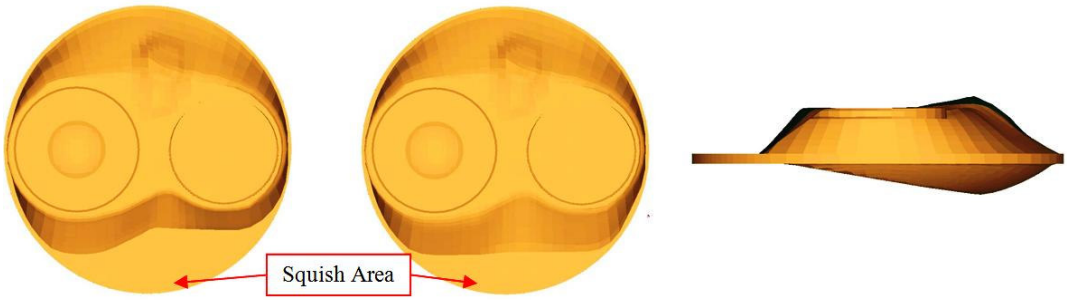

Fig.2

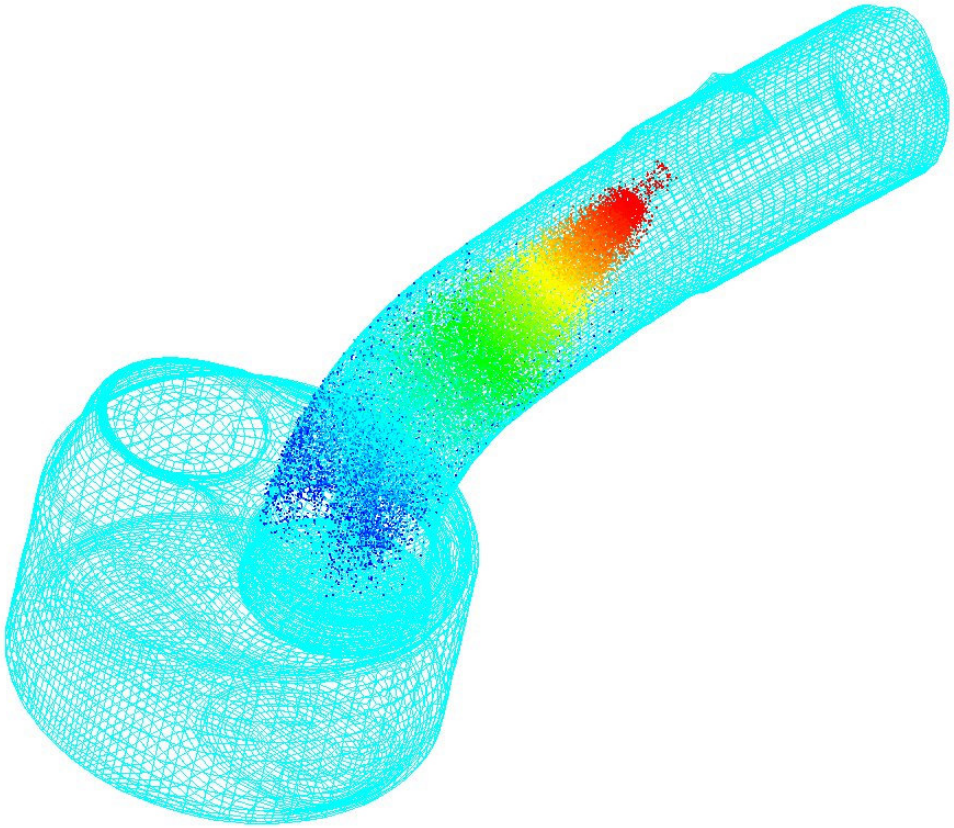

Fig.3

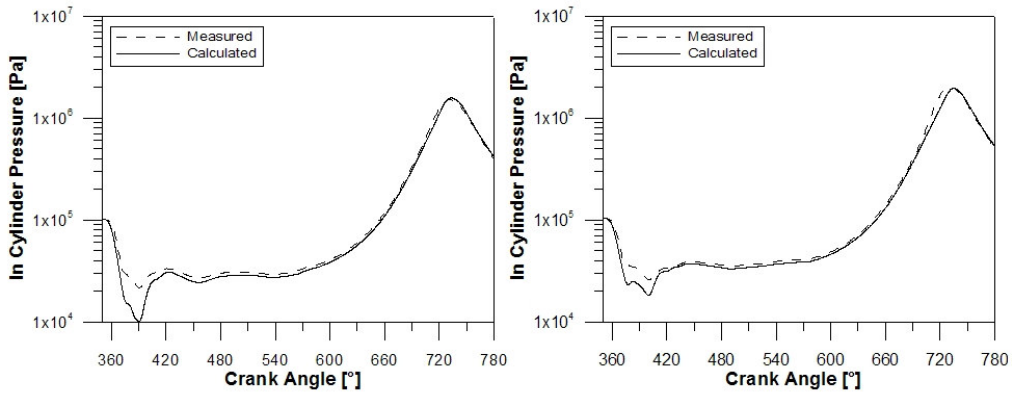

Fig.4

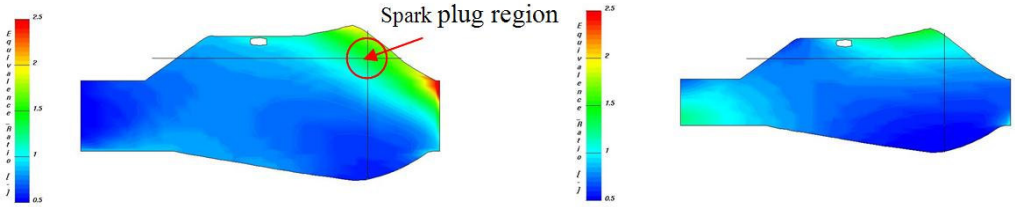

Fig.5

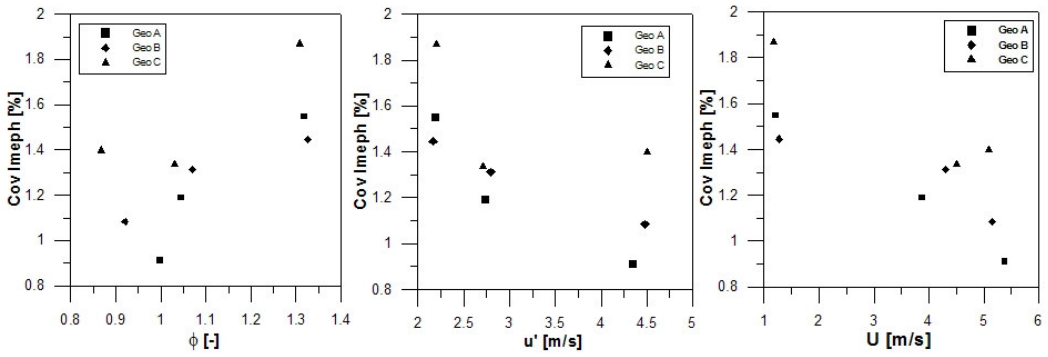

Fig.6

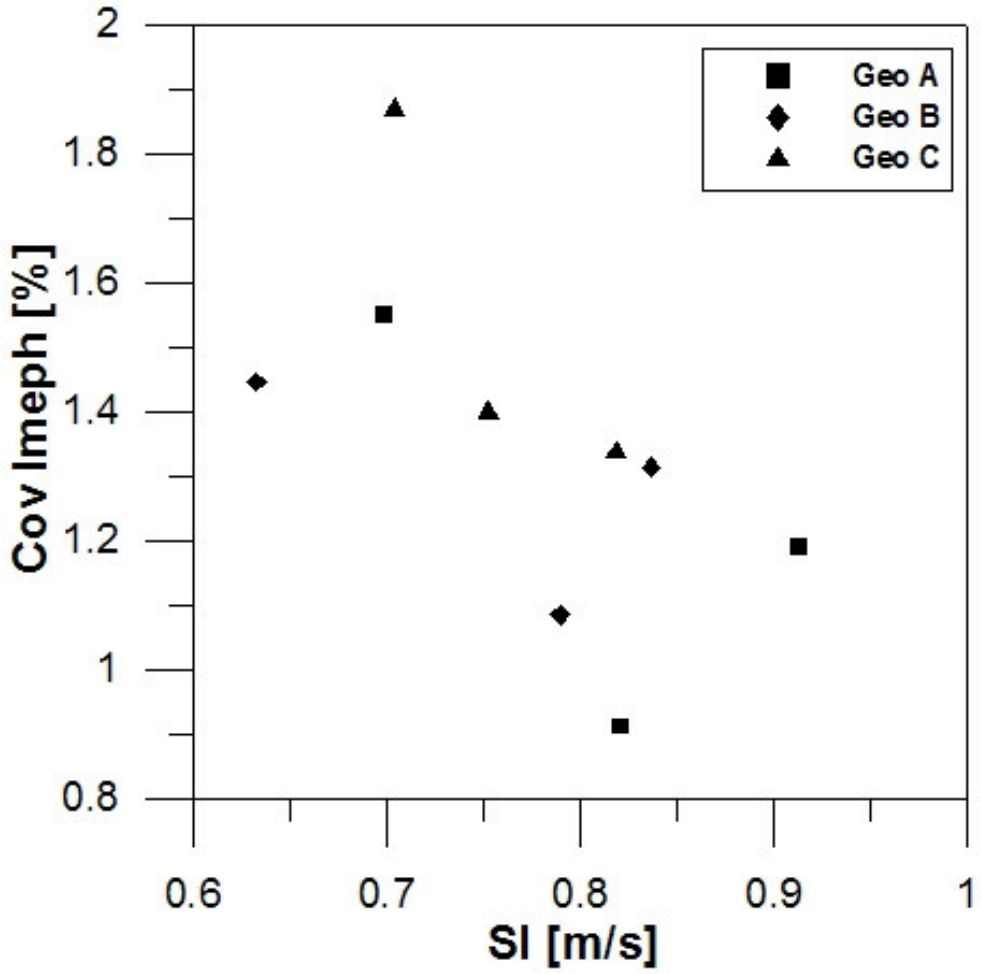

Fig.7